

Improved constraint on primordial gravitational waves in light of the Hubble tension and BICEP/Keck

Gen Ye^{1*} and Yun-Song Piao^{1,2,3,4†}

¹ *School of Physics, University of Chinese Academy of Sciences, Beijing 100049, China*

² *School of Fundamental Physics and Mathematical Sciences, Hangzhou Institute for Advanced Study, UCAS, Hangzhou 310024, China*

³ *International Center for Theoretical Physics Asia-Pacific, Beijing/Hangzhou, China and*

⁴ *Institute of Theoretical Physics, Chinese Academy of Sciences, P.O. Box 2735, Beijing 100190, China*

Abstract

The Hubble tension that the standard Λ CDM model is suffering from can be resolved with pre-recombination early dark energy. We present the first constraint on the tensor-to-scalar ratio r in corresponding Hubble-tension-free cosmologies using the most recent BICEP/Keck cosmic microwave background (CMB) B-mode polarization data. We find, combining BICEP/Keck with Planck18 CMB and baryon acoustic oscillation data, that the models with larger Hubble constant H_0 will have tighter upper bound on r , and resolution $H_0 \sim 73$ km/s/Mpc of the Hubble tension tightens the upper bound to $r < 0.028$ (95% C.L.), 25% tighter than the Λ CDM constraint $r < 0.036$. We clarify the origin of this tightening bound.

PACS numbers:

* yegen14@mailsucas.ac.cn

† yspiao@ucas.ac.cn

I. INTRODUCTION

Inflation is the current paradigm of early universe [1–4]. It predicts nearly scale-invariant scalar perturbation, which is consistent with the cosmic microwave background (CMB) observations, as well as the constraint on primordial gravitational waves (GWs). The discovery of primordial GWs will solidify our confidence that inflation has ever happened. The primordial GWs will source B-mode polarization in the CMB [5–7], which is currently the most promising way to search for the primordial GWs.

Based on the standard Λ CDM model, combining Planck18 and BICEP/Keck15 data the Planck collaboration has put the constraint on the tensor-to-scalar ratio, $r < 0.066$ (95% C.L.) [8]. Recently, combining Planck18, baryon acoustic oscillations (BAO) and latest BICEP/Keck18 data the BICEP/Keck collaboration has lowered the upper bound to $r < 0.036$ (95% C.L.) [9]¹. However, it is well-known that the Λ CDM model suffers the Hubble tension, i.e. the locally measured value of current expansion rate reported by the SH0ES collaboration is $H_0 \sim 73.04 \pm 1.04 \text{ km/s/Mpc}$ [11], in stark ($\sim 5\sigma$) tension with $H_0 = 67.37 \pm 0.54 \text{ km/s/Mpc}$ [8] inferred by the Planck collaboration assuming Λ CDM.

Though the possibility of some unknown systematics in data causing this tension [12] cannot be ruled out, the Hubble tension is actually becoming a pointer to new physics beyond Λ CDM, see e.g. [13, 14] for reviews. The inclusion of early dark energy (EDE) [15], see also [16–24], has proved to be a promising route of resolving the Hubble tension. In Hubble-tension-free EDE cosmologies, the bestfit values of cosmological parameters have shifted notably in correlation with the increment in H_0 [25], see also [26–29]. The parameter shifts can serve as tests of corresponding EDE models, which have been confronted with large scale structure data [26, 30, 31] and high- l CMB data from ground based experiments [32–37], respectively.

The amplitude A_s , tilt n_s of primordial scalar perturbations and the tensor-to-scalar ratio r set the initial condition of CMB. They are converted into the observed CMB anisotropies through perturbation evolution described by a certain cosmological model. Thus it is to be expected that any constraints on the relevant parameters acquired assuming Λ CDM will get modified in the new cosmologies. It has been found in [25] that the shift of primordial scalar

¹ A slightly tighter bound $r < 0.032$ is obtained using the new Planck PR4 data [10].

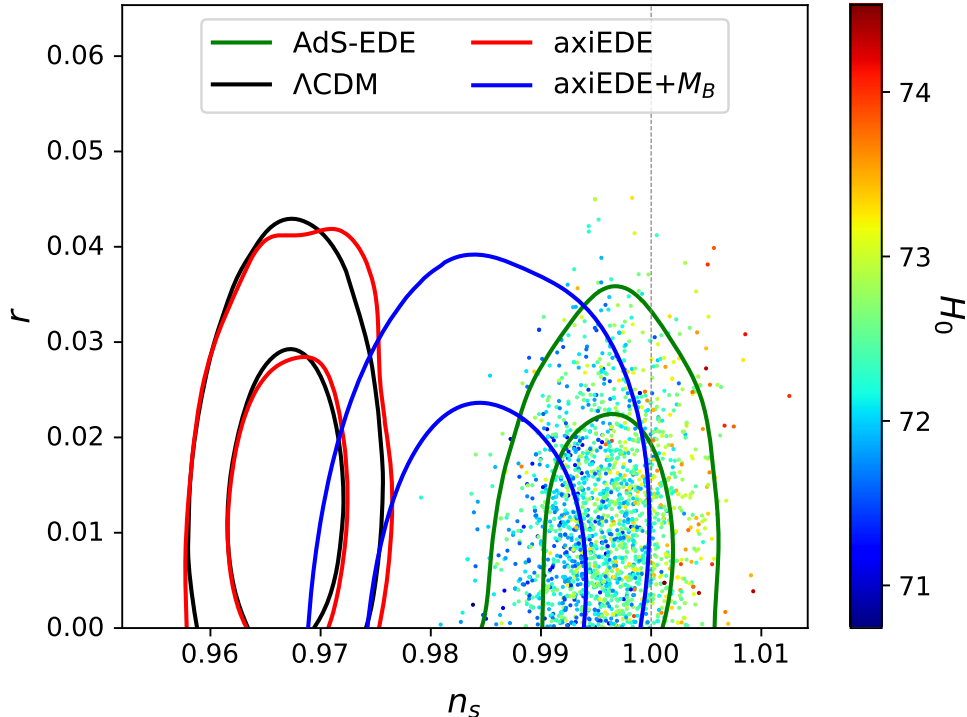


FIG. 1: 68% and 95% C.L. contour plot of the tensor-to-scalar ratio r versus the primordial scalar spectrum tilt n_s , with a color coding for H_0 . All EDE results include the dataset P18+BK18+BAO+SN, while axiEDE+ M_B additionally includes the SH0ES result as a Gaussian prior on the absolute magnitude calibration M_B [38, 39]. The Λ CDM result is from Ref.[9] with the dataset P18+BK18+BAO. Generally, the EDE models with larger H_0 have larger n_s and tighter upper bound on r . Resolution of the Hubble tension ($H_0 \sim 73$ km/s/Mpc) roughly corresponds to $n_s \approx 1$ Ref.[25] and a 25% tighter r upper bound, see (2).

spectral index scales as

$$\delta n_s \simeq 0.4 \frac{\delta H_0}{H_0}, \quad (1)$$

and so the Hubble-tension-free cosmologies actually suggests a scale-invariant Harrison-Zeldovich primordial scalar spectrum, i.e. $n_s = 1$ for $H_0 \sim 73$ km/s/Mpc. $n_s = 1$ have profound implication on inflation and primordial Universe, see e.g. recent Refs.[40, 41].

In view of the inevitability of Hubble tension in Λ CDM [42], it is significant and also imperative to constrain r in Hubble-tension-free cosmologies, e.g.[15, 21], using the most recent BICEP/Keck B-mode polarization data. In this Letter, we will present the first constraint on r in corresponding cosmologies. We find that the models predicting larger H_0

will have larger n_s and tighter upper bound on r , and resolution $H_0 \sim 73\text{km/s/Mpc}$ of the Hubble tension tightens the upper bound on r to

$$r < 0.028 \text{ (95\%C.L.)}, \quad (2)$$

25% tighter than the ΛCDM constraint $r < 0.036$ reported by the BICEP/Keck collaboration [9], see Fig.1. We clarify the origin of this tightening bound², and comment on the possibility to relax it.

II. MODEL AND DATA

As concrete examples of Hubble-tension-free cosmologies, we limit ourself to the EDE, which must be non-negligible only for a short epoch decades before recombination and can be implemented as a canonical scalar field ϕ with a potential $V(\phi)$. The EDE models we consider will be: axion-like EDE [15] with an oscillating potential $V(\phi) = m^2 f_a^2 (1 - \cos(\phi/f_a))^n$ and $n = 3$ (denoted as axiEDE for simplicity), and AdS-EDE [21] with a rolling potential $V(\phi) = V_0 (\frac{\phi}{M_p})^4 - V_{ads}$ glued to a cosmological constant $V(\phi) = \text{const.} > 0$ at $\phi = (\frac{V_{ads}}{V_0})^{1/4} M_p$, where V_{ads} is the depth of anti-de Sitter (AdS) well. The evolution of Universe after recombination is ΛCDM -like, see also e.g.[44].

We use modified versions³ of CLASS [45, 46] to compute cosmology and the MontePython-3.4 sampler [47, 48] to perform Monte Carlo Markov Chain (MCMC) analysis. In addition to the six ΛCDM parameters $\{\omega_b, \omega_{cdm}, H_0, \ln 10^{10} A_s, n_s, \tau_{reion}\}$, we vary two additional MCMC parameters $\{\ln(1 + z_c), f_{ede}\}$, with z_c being the redshift at which the field ϕ starts rolling and f_{ede} the energy fraction of EDE at z_c , for both EDE models. The axiEDE model varies yet one more MCMC parameter $\Theta_i \equiv \phi_i/f_a$, the initial position of the field. We set $n_T = 0$ following BK18 [9].

Our datasets include:

- **P18:** Planck 2018 high- l TTTEEE, low- l TT and EE BB likelihoods as well as Planck lensing [49].

² Using the BICEP/Keck15 data [43], Ref.[25] found the upper bounds on r in EDE to be similar to that in ΛCDM . However, the situation is different with sufficiently precise B-mode data.

³ The corresponding cosmological codes are available at: axiEDE (<https://github.com/PoulinV/AxiCLASS>) and AdS-EDE (https://github.com/genye00/class_multiscf).

- **BK18:** The most recent CMB B-mode polarization data from BICEP/Keck 2018 [9].
- **BAO:** Post-reconstructed BAO measurements from 6dF [50], MGS [51] and BOSS DR12 [52].
- **SN:** the Pantheon dataset, with a single nuisance parameter M_B , calibrating the absolute magnitude of the supernovas [53].

In the following we also include the standard Λ CDM model for reference. However, we do not redo the MCMC analysis for the Λ CDM model but directly use the Λ CDM chains from BK18 ⁴ [9] (P18+BK18+BAO).

III. RESULTS AND DISCUSSION

The MCMC posterior results of $\{H_0, n_s, r\}$ for the Λ CDM and EDE models are presented in Table.I and Fig.2, see appendix-A for the results of all relevant parameters. Here, what we intend to discuss is the tighter upper bound on the tensor-to-scalar ratio r . In Fig.2, we see that in EDE models the upper bound on r becomes tighter as H_0 increases, and with AdS-EDE ($H_0 = 72.36_{-0.56}^{+0.49}$ km/s/Mpc) we have the tightest bound $r < 0.028$, roughly 25% lower than the Λ CDM bound. The origin of this result is quite complicated, which we will clarify step by step.

We plot the bestfit total B-mode power spectra $C_{l,tot}^{BB}$, the separate contribution from lensing B-mode $C_{l,lensing}^{BB}$ and tensor $C_{l,tensor}^{BB}$, as well as binned data points in Fig.3. The difference in r is obvious and the Λ CDM (dashed black) and AdS-EDE lines for $C_{l,tot}^{BB}$ are easily distinguishable in Fig.3, despite both fit the BK18 data equally well according to Table.II. Reducing n_s in AdS-EDE to its Λ CDM bestfit value (solid cyan) yields nearly identical results to the AdS-EDE bestfit (dotted green) in Fig.3, **thus n_s is not directly relevant to the change in the upper bound of r .**

The difference in upper bound is related to the different bestfit values of r in Λ CDM and EDE. In Fig.4, we plot the response of total BK18 χ^2 to the variation in r in Λ CDM and AdS-EDE, respectively. It is clear that the χ_{BK}^2 responds to r above the bestfit point very similarly in both models, thus the difference in their bestfit values are carried

⁴ Available at http://bicepkeck.org/bk18_2021_release.html

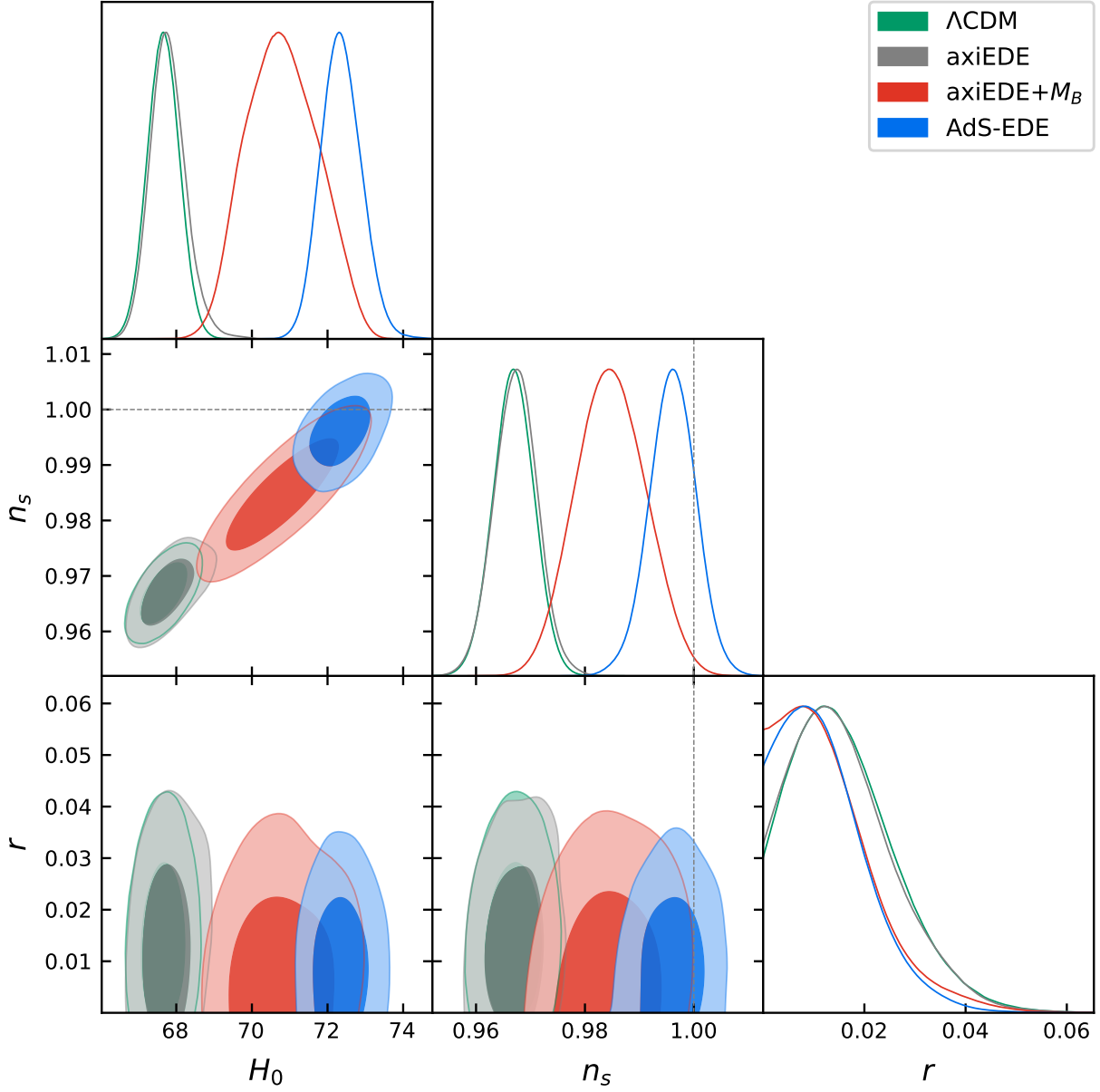


FIG. 2: 68% and 95% posterior distribution of the Λ CDM, axiEDE(w/ and w/o M_B prior) and AdS-EDE models. The Λ CDM contours are produced using the publicly available BK18 chains. Gray bands represent the 1σ and 2σ regions of the SH0ES measurement $H_0 = 73.04 \pm 1.04$ km/s/Mpc. $n_s = 1$ is marked by dotted lines.

over to the derived 95% C.L. upper bounds, i.e. in Table.I the difference in r upper bounds between Λ CDM and EDE is approximately equal to the difference in the corresponding bestfit values for both EDE models.

The increase of power in $C_{l,lensing}^{BB}$ (see the dotted green and dashed black lines

Parameter	Λ CDM	axiEDE (w/o M_B prior)	axiEDE (w/ M_B prior)	AdS-EDE
$100\omega_b$	$2.242(2.231) \pm 0.013$	$2.239(2.276)_{-0.016}^{+0.013}$	$2.291(2.281) \pm 0.023$	$2.334(2.343) \pm 0.017$
ω_{cdm}	$0.1193(0.1195) \pm 0.0009$	$0.11983(0.1248)_{-0.0013}^{+0.0009}$	$0.1270(0.1302) \pm 0.0035$	$0.1342(0.1327) \pm 0.0018$
τ_{reio}	$0.0565(0.0526) \pm 0.0073$	$0.0562(0.0642)_{-0.0075}^{+0.0067}$	$0.0542(0.0551) \pm 0.0074$	$0.0535(0.0552) \pm 0.0077$
H_0	$67.66(67.57) \pm 0.42$	$67.78(70.02)_{-0.50}^{+0.41}$	$70.82(71.83)_{-1.0}^{+0.90}$	$72.36(72.44)_{-0.56}^{+0.49}$
$\ln 10^{10} A_s$	$3.048(3.036) \pm 0.014$	$3.045(3.077) \pm 0.015$	$3.091(3.073)_{-0.015}^{+0.019}$	$3.070(3.071) \pm 0.015$
n_s	$0.9669(0.9658) \pm 0.0037$	$0.9673(0.9868) \pm 0.0039$	$0.9848(0.9907) \pm 0.0063$	$0.9961(0.9978) \pm 0.0043$
r	$< 0.035(0.015)$	$< 0.035(0.011)$	$< 0.031(0.011)$	$< 0.028(0.008)$
f_{ede}	–	$< 0.024(0.070)$	$0.075(0.116)_{-0.035}^{+0.019}$	$0.1120(0.1062)_{-0.0076}^{+0.0040}$
$\ln(1 + z_c)$	–	$8.50(8.81) \pm 0.63$	$8.090(8.258)_{-0.18}^{+0.083}$	$8.189(8.178) \pm 0.079$
Θ_i	–	$1.68(2.97)_{-0.73}^{+1.3}$	$1.65(2.76)_{-0.57}^{+0.30}$	–
Ω_m	$0.3111(0.3119) \pm 0.0057$	$0.3110(0.3022) \pm 0.0054$	$0.3002(0.2978)_{-0.0056}^{+0.0048}$	$0.3021(0.2976) \pm 0.0054$
S_8	$0.826(0.823) \pm 0.010$	$0.825(0.832) \pm 0.010$	$0.843(0.836)_{-0.010}^{+0.013}$	$0.858(0.849) \pm 0.011$

TABLE I: Bestfit (in parenthesis) and 68% C.L. marginalized constraints (for one-sided bounds the 95% result is given) on the cosmological parameters of the Λ CDM and EDE models. The Λ CDM constraints are calculated from the publicly available BK18 chains with the dataset P18+BK18+BAO. The axiEDE and AdS-EDE results are obtained using the dataset P18+BK18+BAO+SN, and axiEDE with M_B prior also include the SH0ES result as a Gaussian prior on the absolute magnitude calibration M_B .

in Fig.3) is a major contributing factor to the difference in the bestfit values of r between EDE and Λ CDM. It remains to understand why such distinct values of r , i.e. $r = 0.015$ for Λ CDM and $r = 0.008$ for AdS-EDE, can fit the BK18 data equally well. To this end, we perform a crude data cut to BK18 - using only part of BK18's nine l -bins (corresponding to the nine data points in Fig.3) to calculate χ^2 . The results are plotted in Fig.5. Overall it is the first three bins ($l = 37 - 120$) that are most sensitive to the variation in r since they contribute most of the change in $\Delta\chi_{BK}^2$. The first bin favors (i.e. smallest $\Delta\chi_{BK}^2$) non-zero r . On the other hand, large r lines peak at the second bin while the line with the smallest $r = 0.001$ (blue) displays the deepest dip there, showing a preference for $r \lesssim 0.001$. Bin #3 on the other hand prefers $r \gtrsim 0.04$.

Bin #3 ($l = 91 - 120$) is much less sensitive (i.e. smaller increment in $\Delta\chi_{BK}^2$ for $r < 0.001$

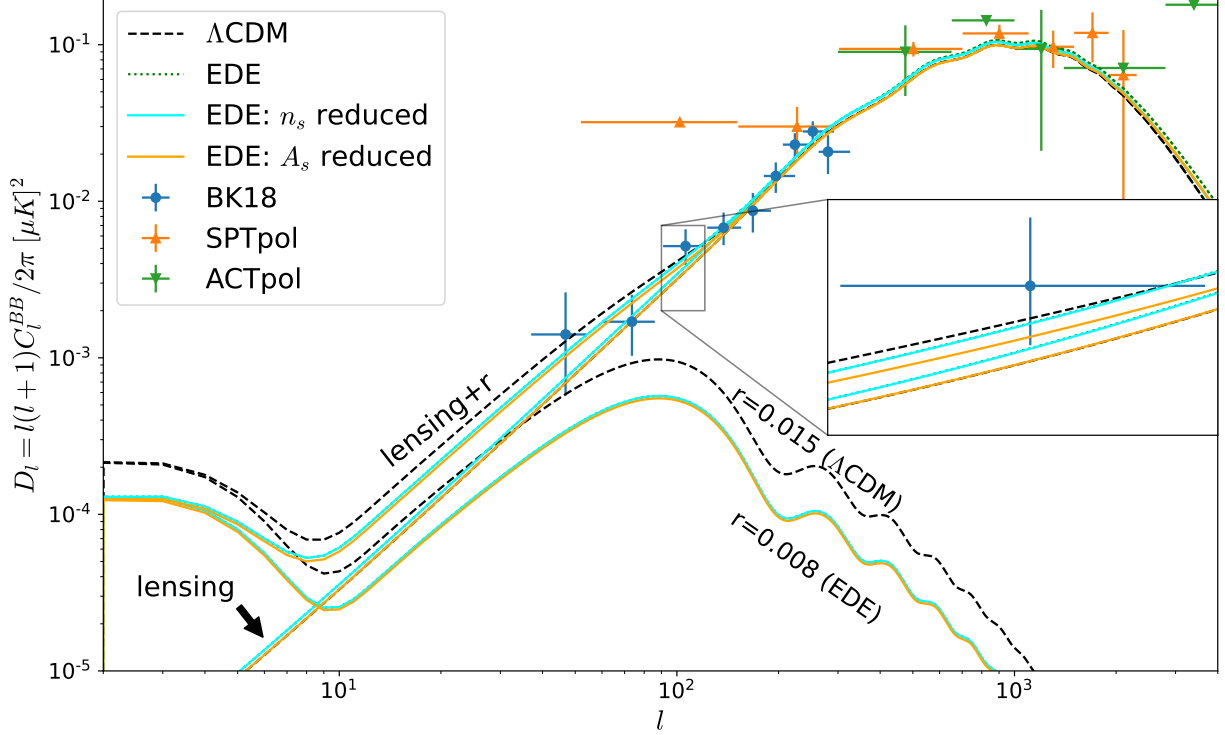


FIG. 3: $C_{l,tot}^{BB}$, $C_{l,lensing}^{BB}$ and $C_{l,tensor}^{BB}$ with different color and line style for the bestfit Λ CDM (dashed black), bestfit AdS-EDE (dotted green) and bestfit AdS-EDE but with A_s (solid orange) or n_s (solid cyan) set to their Λ CDM bestfit values. Points with error bars are binned BK18 [9], SPT [54] and ACT [55] data points. The n_s -reduced AdS-EDE lines are nearly identical to those of AdS-EDE bestfit thus the dotted green lines overlap with the cyan ones and are barely visible.

in Fig.5) to small r in EDE⁵, which suggests that a much smaller r is allowed to fit bin #2 better without significantly worsening the fit at bin #3. $C_{l,tot}^{BB}$ in EDE and Λ CDM are actually well constrained by BK18 data near bin #3, see the zoomed-in region of Fig.3, both bestfit lines very close to each other and intersecting. **In the bestfit Λ CDM, $C_{l,lensing}^{BB}$ contributes roughly 80% power of the total amplitude near $l = 100$, thus the 10% increase, see Fig.6, in $C_{l,lensing}^{BB}$ from Λ CDM to EDE needs a 50% reduction in $C_{l,tensor}^{BB}$ to keep $C_{l,tot}^{BB} = C_{l,tensor}^{BB} + C_{l,lensing}^{BB}$ approximately unchanged, corresponding to a 50% reduction in r bestfit, i.e. $\delta r \sim 0.007$.** It is surprising that this rather crude estimate explains the difference in bestfit values of r in Table.I pretty well.

⁵ The same applies to bin #1, but the constraining power on r comes mostly from bin #3 due to its higher data quality.

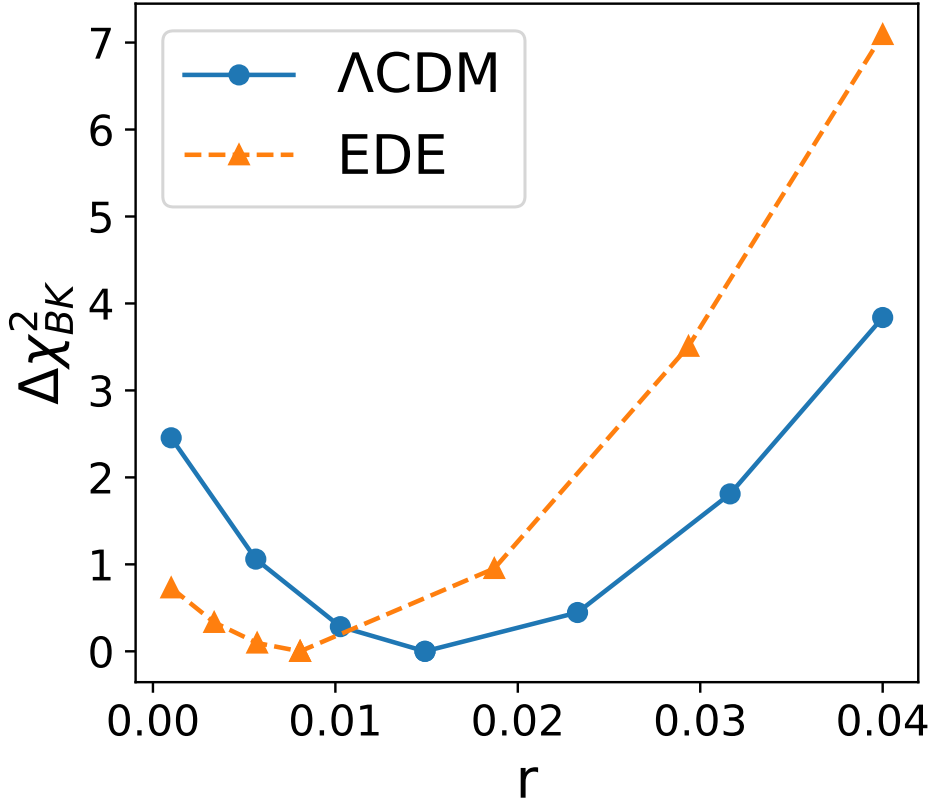


FIG. 4: Response of total BK18 χ^2 to the variation in r in Λ CDM and AdS-EDE. χ^2 at each point is calculated by varying r with all other parameters, including nuisance, fixed to their bestfit values. The y -axis plots $\Delta\chi^2 = \chi^2 - \chi_{bestfit}^2$ for the BK18 dataset.

One of the sources of the enhanced $C_{l,lensing}^{BB}$ in EDE is an excess of power in $C_l^{\phi\phi}$ at $l = 200 - 800$, away from its primary peak. We compare the $C_{l,lensing}^{BB}$ brought by different $C_l^{\phi\phi}$ from different unlensed C_l^{EE} in Fig.6. We set $A_L = 1$ throughout this paper. It is clear from Fig.6(a) that the enhancement in $C_{l,lensing}^{BB}$ nearly entirely comes from the difference in $C_l^{\phi\phi}$. This is understandable since C_l^{EE} (lensed) in both bestfit models are tightly constrained by the Planck data, and so nearly the same. The major contribution to the difference in $C_{l,lensing}^{BB}$ between Λ CDM and AdS-EDE comes from $C_l^{\phi\phi}$ ($200 < l < 800$), see Fig.6(b). Interestingly, the peak of $C_l^{\phi\phi}$ (related to the peak of the matter power spectrum P_k , corresponding to scales entering horizon near matter-radiation equality) is excluded from this multiple range. It also explains why in Fig.3 changing n_s has nearly no effect on the lensing B-mode, since $200 < l < 800$ is near the pivot scale $k_{pivot} = 0.05\text{Mpc}^{-1}$ which is

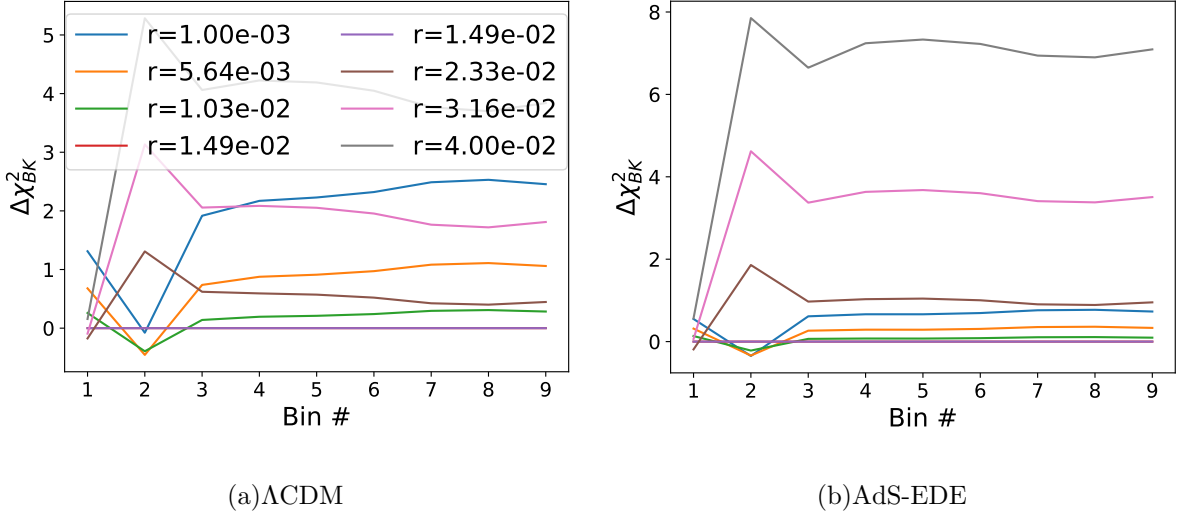


FIG. 5: $\Delta\chi^2 = \chi^2 - \chi^2_{best\,fit}$ for BK18 with data cuts. The x -axis represents that only the first x bins (counting from low- l) out of the total nine l -bins of BK18 are used in the calculation of χ^2 and y -axis for the difference in BK18 χ^2 compared with the bestfit model with the same data cuts. Complete BK18 dataset corresponds to bin $\#$ =9 on the horizontal axis.

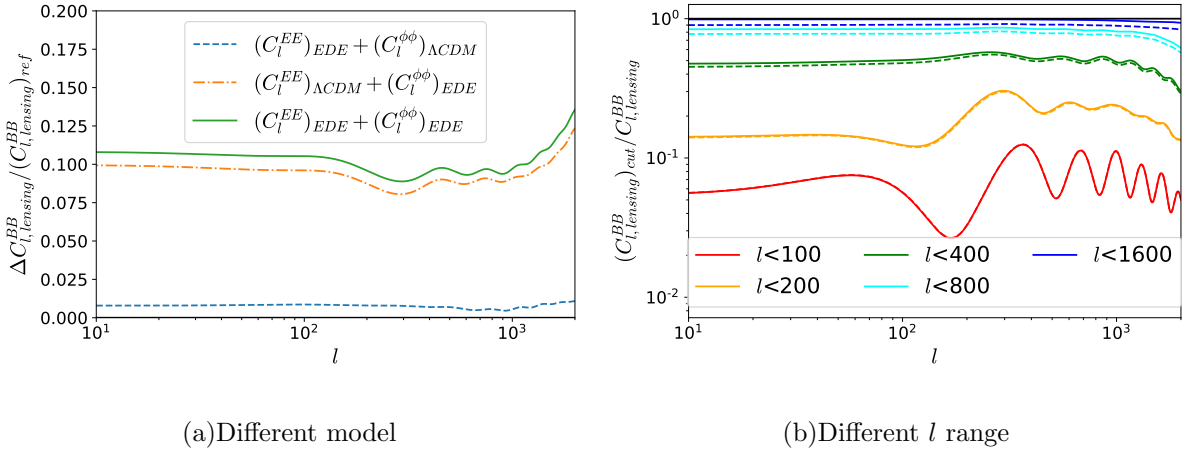


FIG. 6: The lensing B-mode calculated using different $C_l^{\phi\phi}$ and C_l^{EE} . *Left panel:* Relative difference in $C_{l,lensing}^{BB}$ compared with Λ CDM bestfit. Results are calculated using different combination of unlensed C_l^{EE} and $C_l^{\phi\phi}$ from the Λ CDM and AdS-EDE bestfit model. *Right panel:* $C_{l,lensing}^{BB}$ calculated from bestfit AdS-EDE unlensed C_l^{EE} , using different portion of the $C_l^{\phi\phi}$ from the same model, compared with the full lensing C_l^{BB} .

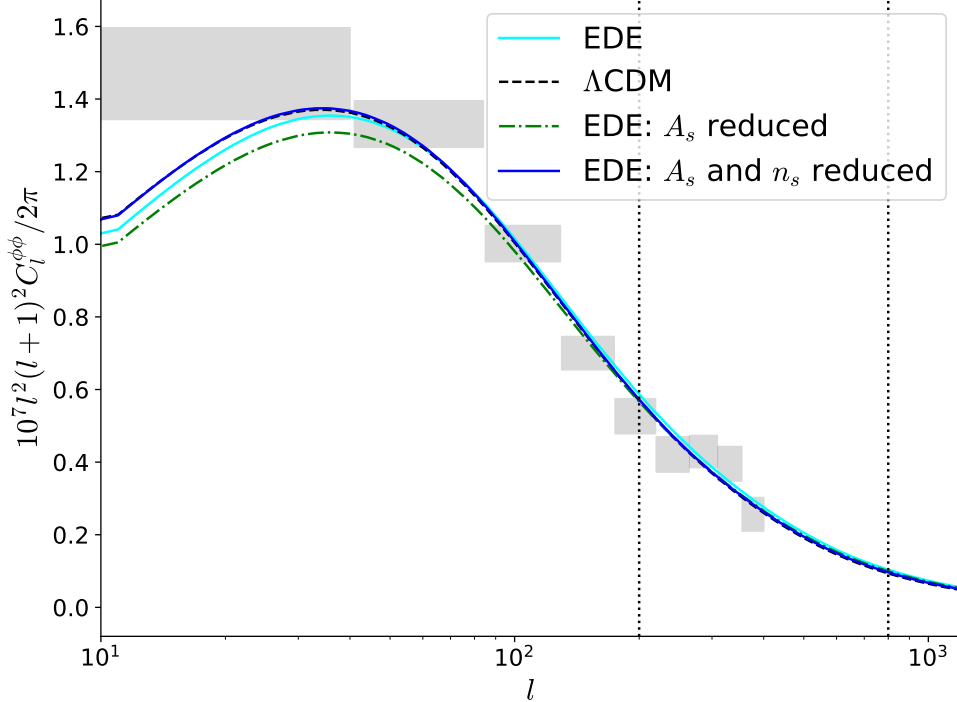


FIG. 7: The lensing convergence spectrum $C_l^{\kappa\kappa} = l^2(l+1)^2 C_l^{\phi\phi}/4$ in the bestfit Λ CDM and AdS-EDE models. AdS-EDE models with A_s and/or n_s set to their Λ CDM bestfit values are also plotted. The vertical dotted lines mark the position of $l = 200$ and $l = 800$. The gray shaded regions are the band power constraints from Planck18 lensing reconstruction [56]. Comparing the solid blue and green dashed dotted lines, changing n_s affects the peak (away from pivot) but not the region $200 < l < 800$ (near the pivot).

much more sensitive to A_s rather than n_s .

We attribute the additional power in $C_l^{\phi\phi}(200 < l < 800)$ to the increment in ω_{cdm} and A_s , which enhances amplitude of the matter power spectrum P_k on all scales smaller than k_{eq} , the peak of P_k , so $C_l^{\phi\phi}(200 < l < 800)$. On the other hand, for EDE, the increment in ω_{cdm} in fact has minor effect on the peak (located near $l \sim 60$) height of $C_l^{\phi\phi}$, see appendix-B for details. The shift (1) of n_s suppresses power at $l \sim 60$ by $1 - (l_{peak}/l_{pivot})^{\delta n_s} \sim 1 - (60/500)^{0.03} \approx 6\%$ but does not obviously affect $200 < l < 800$ which is near $l_{pivot} \simeq 500$. AdS-EDE brings nearly identical $C_l^{\phi\phi}$ near $l \lesssim 100$ as Λ CDM does under the same initial condition. To compensate for the power deficit at the lensing peak $l \simeq 60$ caused by increasing n_s , the amplitude A_s has been slightly increased in AdS-

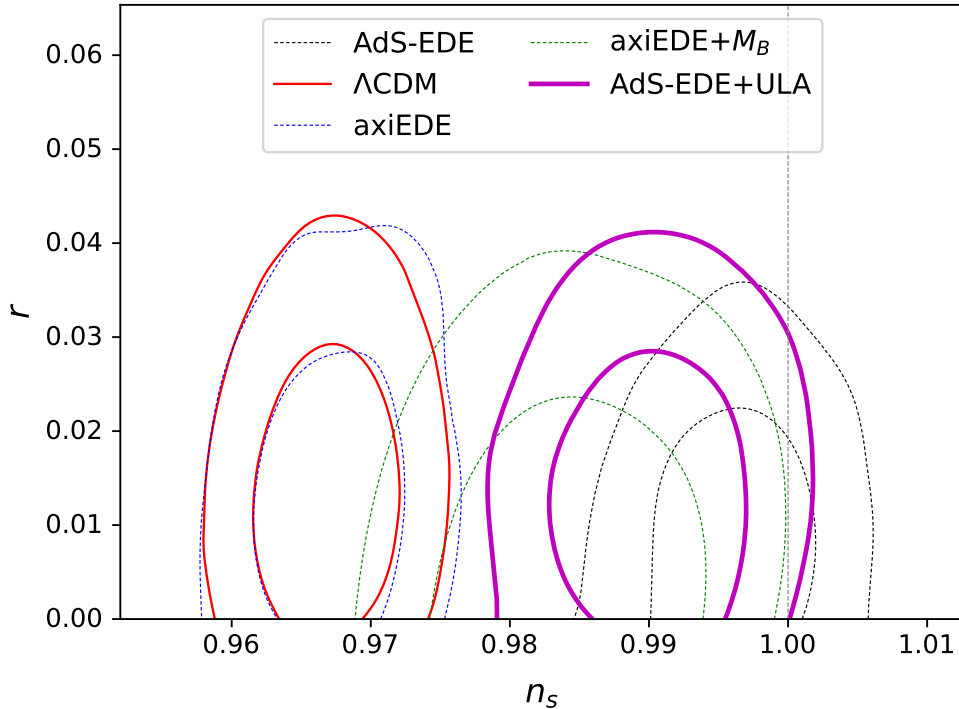


FIG. 8: $r - n_s$ plot highlighting the Λ CDM and AdS-EDE plus ultra light axion (ULA) models. The upper bound on r in AdS-EDE+ULA is relaxed to be comparable with Λ CDM.

EDE, which further enhances $C_l^{\phi\phi}$ in the relevant multiple range $200 < l < 800$. The above observation about n_s and A_s has been confirmed in Fig.7.

As clarified, it is the enhanced matter power spectrum, so lensing potential $C_{l,lensing}^{BB}$, at $l > 200$ that results in the tightened bound on r . Thus suppressing matter power spectrum on small scales will possibly relax the bound, which might be relevant with resolving S_8 tension. As a cross check, we confront the AdS-EDE plus ultra light axion model [57] (able to restore cosmological concordance with both S_8 and H_0) with P18+BK18+BAO+SN dataset as well as the Gaussian prior $S_8 = 0.755^{+0.019}_{-0.021}$ [58], and plot the MCMC results in Fig.8. As expected, the constraints on r is relaxed to $r < 0.034$ (95%C.L.) (but still $n_s \approx 1$), comparable to the Λ CDM result $r < 0.035$ (95%C.L.).

IV. CONCLUSION

We present the first constraint on primordial GWs, quantified as the tensor-to-scalar ratio r , in Hubble-tension-free EDE cosmologies using the most recent BK18 data. It is found

that the upper bound on r gets tightened in correlation with the increment in H_0 , and the most stringent bound $r < 0.028$, as opposed to $r < 0.036$ reported by the BICEP/Keck collaboration for Λ CDM [9], is obtained using the EDE model with the largest Hubble constant, i.e. $H_0 = 72.36^{+0.49}_{-0.56}$ km/s/Mpc in AdS-EDE. We argued that this tightening of bound is a manifestation of the competition between $C_{l,tensor}^{BB}$ and $C_{l,lensing}^{BB}$ with $C_{l,tot}^{BB} = C_{l,tensor}^{BB} + C_{l,lensing}^{BB}$ constrained by the BK18 data. In the EDE models, the increment in ω_{cdm} and A_s brings more power at intermediate and small scales ($l > 200$) in the matter power spectrum, enhancing $C_l^{\phi\phi}$ ($200 < l < 800$) and thus $C_{l,lensing}^{BB}$. As a consequence, the $C_{l,tensor}^{BB}$ allowed by BK18 must be lowered, so the smaller r .

Our results underline that the exact upper bound on r is model-dependent even with the most recent BK18 data. The take-away message for primordial Universe model building is that though the order of magnitude constraint from observation $r \lesssim \mathcal{O}(10^{-2})$ is to be respected, detailed value of the bound might be different in different cosmological models, which will have profound implication to inflation and early Universe physics. Our results also highlight the crucial roles of weak lensing from scales $k = \mathcal{O}(0.01 \sim 0.1\text{Mpc}^{-1})$, probed by galaxy surveys such as DES [59] and Euclid [60], in constraining r using BICEP/Keck data, and of accurate measurements of CMB on small scales, with surveys such as Simons Observatory [61] and CMB-S4 [62], in differentiating the Hubble-tension-free cosmologies. It might also be interesting to restudy A_L with the BK18 data [9] in beyond Λ CDM cosmologies which modify $C_l^{\phi\phi}$.

Acknowledgments This work is supported by the NSFC, No.12075246, the KRPCAS, No.XDPB15. We acknowledge the Tianhe-2 supercomputer for providing computing resources. Some figures are generated using GetDist [63]. We thank Alessandra Silvestri for useful comments and discussions.

Appendix A: More MCMC results

Table.I and Fig.9 show the posterior results for cosmological parameters. Despite using exactly the same MCMC chains as BK18, we obtained a slightly smaller upper bound $r < 0.035$, which we attribute to different analysis configuration in the GetDist package. Table.II presents the per experiment bestfit χ^2 for each model.

As noted in earlier works, without a $H_0(M_B)$ prior, axiEDE with Planck CMB data on

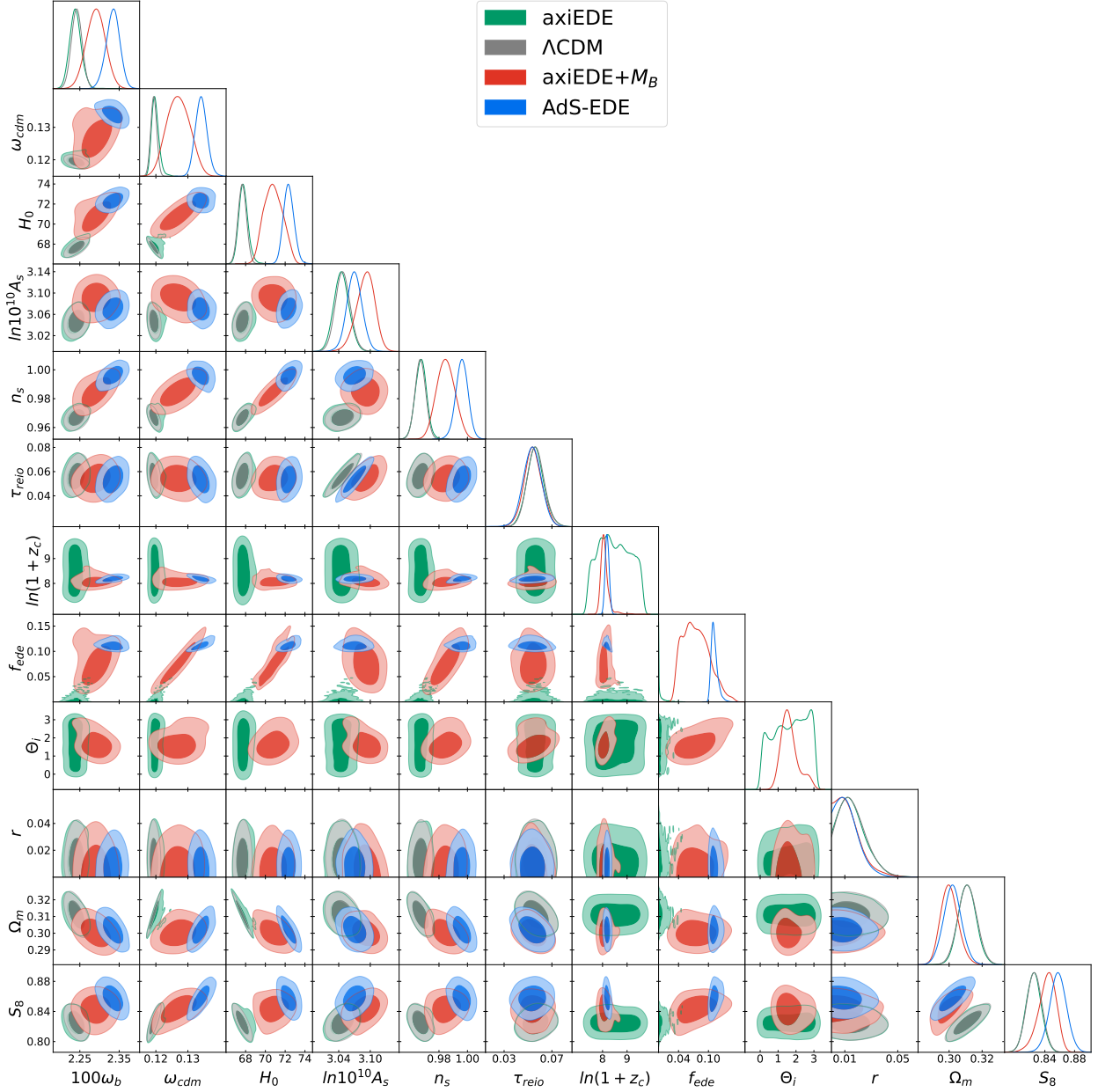


FIG. 9: 68% and 95% posterior distributions of all cosmological parameters in the Λ CDM and EDE models.

its own yields nearly identical results to Λ CDM and f_{ede} is compatible with zero, despite a bestfit point outside the 1σ contours where EDE is non-negligible and H_0 is much larger. This is because both the Λ CDM bestfit ($f_{ede} = 0$) and the EDE bestfit ($f_{ede} \neq 0$) are local minima in the full phase space, but other EDE parameters (such as Θ_i or z_c) are essentially free in the $f_{ede} = 0$ case, thus the phase space around the Λ CDM bestfit viable to the MCMC chain is dimensionally larger than that around the EDE bestfit point. And without

Dataset	Λ CDM	axiEDE (w/o H_0 prior)	axiEDE (w/ H_0 prior)	AdS-EDE
Planck high- l TTTEEE	2349.64	2348.61	2347.00	2348.16
Planck low- l TT	23.61	21.09	21.06	20.54
Planck low- l EE BB	395.90	394.09	392.77	392.74
Planck lensing	8.95	9.60	9.91	11.17
BK18	537.25	536.70	536.01	535.93
BAO	5.78	5.24	5.62	5.46
SN	–	1027.04	1026.86	1026.86
M_B prior	–	–	4.65	–

TABLE II: Bestfit χ^2 for each likelihood. The Λ CDM bestfit is taken to be the point with the lowest total χ^2 value in the publicly available chains by BK18.

any $H_0(M_B)$ -related prior, the EDE bestfit is only marginally better than the Λ CDM one, see χ^2 in axiEDE in Table II, thus the MCMC chain will inevitably center around the Λ CDM local minima, see also [64] for recent discussion.

The AdS-EDE model resolves the Hubble tension even without a $H_0(M_B)$ -related prior partially because the AdS phase masks out the Λ CDM bestfit point since too small f_{ede} will result in the field confined in the disastrous AdS region and is not favored.

Appendix B: CMB lensing constraints in AdS-EDE

As can be seen in Fig. 7, $C_l^{\phi\phi}$ is nearly identical in both AdS-EDE and Λ CDM around its peak under the same initial conditions (i.e. A_s and n_s). This is because in EDE the parameter most relevant to the peak height of $C_l^{\phi\phi}$ is $\Omega_m h^{0.5}$ rather than $\omega_m = \Omega_m h^2$. Using the variable $y = h\chi$, χ being the angular diameter distance, and the Limber approximation, the lensing convergence spectrum $C_l^{\kappa\kappa} = l^2(l+1)^2 C_l^{\phi\phi}/4$ writes

$$C_l^{\kappa\kappa} = \frac{9}{4} \Omega_m^2 h \int_0^\infty dy a^{-2}(y) \hat{g}_L^2(y) P_m \left(k = \frac{l}{\chi} h, \eta(y) \right) \quad (\text{B1})$$

with η the conformal time. The lensing kernel \hat{g}_L with the window function $W(y)$ is

$$\hat{g}_L(y) = \int_y^\infty dy' \left(1 - \frac{y}{y'} \right) W(y'). \quad (\text{B2})$$

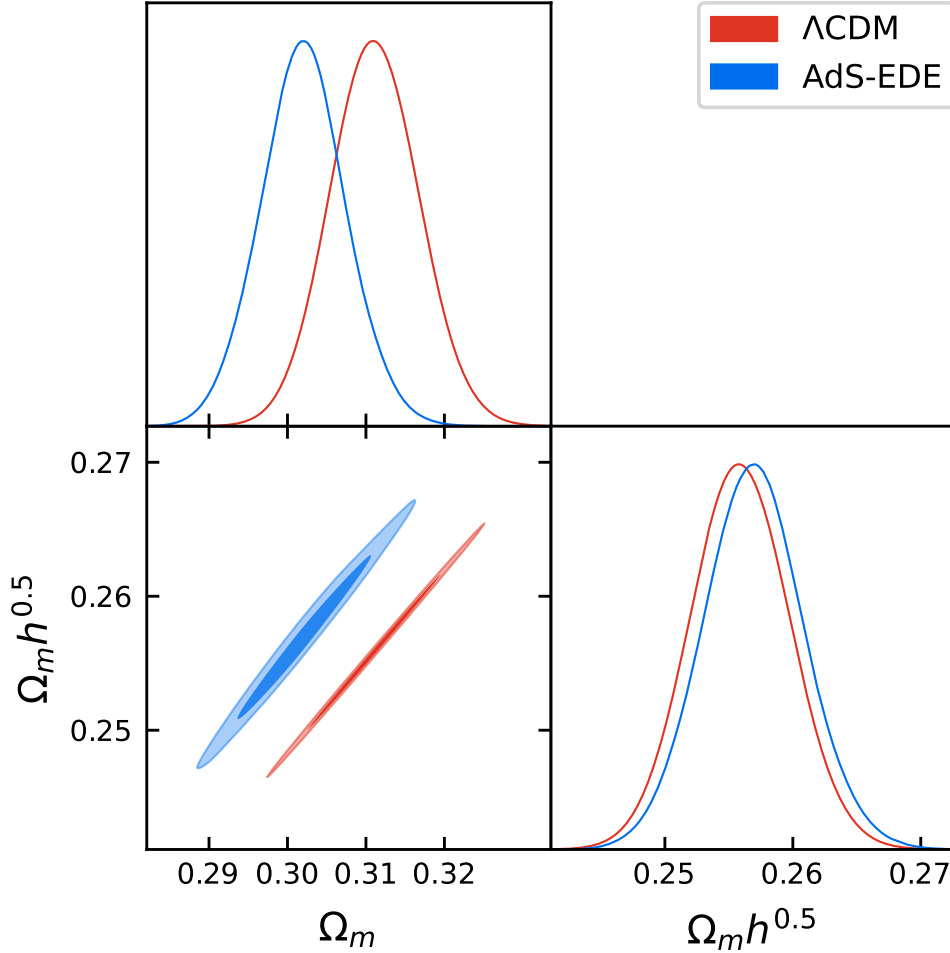


FIG. 10: Posterior distribution of Ω_m versus $\Omega_m h^{0.5}$.

The angular location of the matter power spectrum peak (l_{eq}) is constrained by CMB data in EDE [15] as well as its peak height. Thus the peak height of $C_l^{\kappa\kappa}$ is relevant to the prefactor $\Omega_m h^{0.5}$ in (B1). The Planck lensing reconstruction therefore constrains $\Omega_m h^{0.5} \sim const.$, which is nearly invariant across both models in Fig.10, while Ω_m show some difference. Note this observation does not contradict the result of Ref.[27], in which $\Omega_m \sim const.$ is the background level CMB+BAO constraint. In the actual analysis, since there is residual freedom in both data constraints, the MCMC results make a compromise between different datasets. Thus the actual degeneracy direction is

$$\Omega_m \sim h^{-\alpha}, \quad 0 < \alpha < 0.5, \quad (\text{B3})$$

or equivalently $\omega_m \sim h^\beta$ with $1.5 < \beta < 2$. As an example, numerical principle component analysis of the AdS-EDE chain yields $\Omega_m h^{0.4} \sim \text{const.}$, so $\alpha = 0.4$ and $\beta = 1.6$.

-
- [1] A. H. Guth, Phys. Rev. D **23**, 347 (1981).
 - [2] A. D. Linde, Phys. Lett. B **108**, 389 (1982).
 - [3] A. Albrecht and P. J. Steinhardt, Phys. Rev. Lett. **48**, 1220 (1982).
 - [4] A. A. Starobinsky, Phys. Lett. B **91**, 99 (1980).
 - [5] U. Seljak, Astrophys. J. **482**, 6 (1997), astro-ph/9608131.
 - [6] M. Kamionkowski, A. Kosowsky, and A. Stebbins, Phys. Rev. Lett. **78**, 2058 (1997), astro-ph/9609132.
 - [7] U. Seljak and M. Zaldarriaga, Phys. Rev. Lett. **78**, 2054 (1997), astro-ph/9609169.
 - [8] N. Aghanim et al. (Planck), Astron. Astrophys. **641**, A6 (2020), [Erratum: Astron.Astrophys. **652**, C4 (2021)], 1807.06209.
 - [9] P. A. R. Ade et al. (BICEP, Keck), Phys. Rev. Lett. **127**, 151301 (2021), 2110.00483.
 - [10] M. Tristram et al. (2021), 2112.07961.
 - [11] A. G. Riess et al. (2021), 2112.04510.
 - [12] W. L. Freedman (2021), 2106.15656.
 - [13] E. Di Valentino, O. Mena, S. Pan, L. Visinelli, W. Yang, A. Melchiorri, D. F. Mota, A. G. Riess, and J. Silk (2021), 2103.01183.
 - [14] L. Perivolaropoulos and F. Skara (2021), 2105.05208.
 - [15] V. Poulin, T. L. Smith, T. Karwal, and M. Kamionkowski, Phys. Rev. Lett. **122**, 221301 (2019), 1811.04083.
 - [16] P. Agrawal, F.-Y. Cyr-Racine, D. Pinner, and L. Randall (2019), 1904.01016.
 - [17] S. Alexander and E. McDonough, Phys. Lett. B **797**, 134830 (2019), 1904.08912.
 - [18] M.-X. Lin, G. Benevento, W. Hu, and M. Raveri, Phys. Rev. D **100**, 063542 (2019), 1905.12618.
 - [19] F. Niedermann and M. S. Sloth, Phys. Rev. D **103**, L041303 (2021), 1910.10739.
 - [20] J. Sakstein and M. Trodden, Phys. Rev. Lett. **124**, 161301 (2020), 1911.11760.
 - [21] G. Ye and Y.-S. Piao, Phys. Rev. D **101**, 083507 (2020), 2001.02451.
 - [22] M. Braglia, W. T. Emond, F. Finelli, A. E. Gumrukcuoglu, and K. Koyama, Phys. Rev. D

- 102**, 083513 (2020), 2005.14053.
- [23] T. Karwal, M. Raveri, B. Jain, J. Khoury, and M. Trodden (2021), 2106.13290.
- [24] E. McDonough, M.-X. Lin, J. C. Hill, W. Hu, and S. Zhou (2021), 2112.09128.
- [25] G. Ye, B. Hu, and Y.-S. Piao (2021), 2103.09729.
- [26] J. C. Hill, E. McDonough, M. W. Toomey, and S. Alexander, *Phys. Rev. D* **102**, 043507 (2020), 2003.07355.
- [27] G. Ye and Y.-S. Piao, *Phys. Rev. D* **102**, 083523 (2020), 2008.10832.
- [28] L. Pogosian, G.-B. Zhao, and K. Jedamzik, *Astrophys. J. Lett.* **904**, L17 (2020), 2009.08455.
- [29] S. Vagnozzi (2021), 2105.10425.
- [30] M. M. Ivanov, E. McDonough, J. C. Hill, M. Simonović, M. W. Toomey, S. Alexander, and M. Zaldarriaga, *Phys. Rev. D* **102**, 103502 (2020), 2006.11235.
- [31] G. D’Amico, L. Senatore, P. Zhang, and H. Zheng, *JCAP* **05**, 072 (2021), 2006.12420.
- [32] A. Chudaykin, D. Gorbunov, and N. Nedelko, *JCAP* **08**, 013 (2020), 2004.13046.
- [33] A. Chudaykin, D. Gorbunov, and N. Nedelko, *Phys. Rev. D* **103**, 043529 (2021), 2011.04682.
- [34] J.-Q. Jiang and Y.-S. Piao, *Phys. Rev. D* **104**, 103524 (2021), 2107.07128.
- [35] V. Poulin, T. L. Smith, and A. Bartlett, *Phys. Rev. D* **104**, 123550 (2021), 2109.06229.
- [36] J. C. Hill et al. (2021), 2109.04451.
- [37] A. La Posta, T. Louis, X. Garrido, and J. C. Hill (2021), 2112.10754.
- [38] D. Camarena and V. Marra, *Mon. Not. Roy. Astron. Soc.* **504**, 5164 (2021), 2101.08641.
- [39] G. Efstathiou, *Mon. Not. Roy. Astron. Soc.* **505**, 3866 (2021), 2103.08723.
- [40] F. Takahashi and W. Yin (2021), 2112.06710.
- [41] G. D’Amico, N. Kaloper, and A. Westphal (2021), 2112.13861.
- [42] L. Verde, T. Treu, and A. G. Riess, *Nature Astron.* **3**, 891 (2019), 1907.10625.
- [43] P. A. R. Ade et al. (BICEP2, Keck Array), *Phys. Rev. Lett.* **121**, 221301 (2018), 1810.05216.
- [44] H. Wang and Y.-S. Piao (2022), 2201.07079.
- [45] J. Lesgourgues (2011), 1104.2932.
- [46] D. Blas, J. Lesgourgues, and T. Tram, *JCAP* **07**, 034 (2011), 1104.2933.
- [47] B. Audren, J. Lesgourgues, K. Benabed, and S. Prunet, *JCAP* **02**, 001 (2013), 1210.7183.
- [48] T. Brinckmann and J. Lesgourgues, *Phys. Dark Univ.* **24**, 100260 (2019), 1804.07261.
- [49] N. Aghanim et al. (Planck), *Astron. Astrophys.* **641**, A5 (2020), 1907.12875.
- [50] F. Beutler, C. Blake, M. Colless, D. H. Jones, L. Staveley-Smith, L. Campbell, Q. Parker,

- W. Saunders, and F. Watson, *Mon. Not. Roy. Astron. Soc.* **416**, 3017 (2011), 1106.3366.
- [51] A. J. Ross, L. Samushia, C. Howlett, W. J. Percival, A. Burden, and M. Manera, *Mon. Not. Roy. Astron. Soc.* **449**, 835 (2015), 1409.3242.
- [52] S. Alam et al. (BOSS), *Mon. Not. Roy. Astron. Soc.* **470**, 2617 (2017), 1607.03155.
- [53] D. M. Scolnic et al., *Astrophys. J.* **859**, 101 (2018), 1710.00845.
- [54] J. T. Sayre et al. (SPT), *Phys. Rev. D* **101**, 122003 (2020), 1910.05748.
- [55] S. K. Choi et al. (ACT), *JCAP* **12**, 045 (2020), 2007.07289.
- [56] N. Aghanim et al. (Planck), *Astron. Astrophys.* **641**, A8 (2020), 1807.06210.
- [57] G. Ye, J. Zhang, and Y.-S. Piao (2021), 2107.13391.
- [58] M. Asgari et al., *Astron. Astrophys.* **634**, A127 (2020), 1910.05336.
- [59] T. M. C. Abbott et al. (DES) (2021), 2105.13549.
- [60] S. Ilić et al. (Euclid) (2021), 2106.08346.
- [61] P. Ade et al. (Simons Observatory), *JCAP* **02**, 056 (2019), 1808.07445.
- [62] K. N. Abazajian et al. (CMB-S4) (2016), 1610.02743.
- [63] A. Lewis (2019), 1910.13970.
- [64] L. Herold, E. G. M. Ferreira, and E. Komatsu (2021), 2112.12140.